PROJECT FINAL REPORT

Grant Agreement number:	270588
Project acronym:	AFCIN
Project title:	Structural designs and tests for integration of active flow control concepts on a trailing edge high lift device
Funding scheme:	???
Period covered:	from April 2011 to June 2014

Name of the scientific representative of the projects's co-ordinator: Prof. Dr.-Ing. Peter Horst, TU Braunschweig, Institute of Aircraft Design and Lightweight Structures

Tel.: +49 531 391 9901

Fax: +49 531 391 9904

e-mail: p.horst@tu-bs.de

Project website address: -

Content

1. Executive Summary

This project had one main aim, namely to find a structural solution for a flap with active flow control features like slits in the outer skin and actuators and a plenum inside the structure. The solution was found for exactly the actuator type developed in the parallel **FloCoSys** project. The outer flap design was chosen according to a flap of the FNG wing, but – due to the active flow control features – the flap only needs 70% of the cordwise dimension of the original flap. According to the reduction in this dimension, other dimensions like the thickness also had to be reduced, which means that the space for internal installations is also smaller than for the original flap.

The special challenge of the project was to find a unique concept for such a flap. It is obvious that small slits in the outer skin will result in a damage/fatigue prone design and will result in lower overall stiffness, at least with respect to torsion and shear from bending of thin-walled profiles. The direction of the pulsed airflow with respect to the upper skin of the flap was requested to be 45°. This has a large impact on the internal structural design, since the actuators have to be positioned accordingly.

Many concepts have been discussed for this case. The result was to use a multi-spar concept for most of the flap. This not only offers some manufacturing advantages, but also the chance to use the forward cell of the flap as plenum. In order to combine the use of the forward cell as plenum and the installation of the actuators under 45° results in an unusual spar design in this area. The overall multi-spar design has then been optimized by special structural design code. Sizing of the structure by means of detailed finite element simulations has been performed likewise.

The flap design was – due to the fact that the overall design was only possible by including the new actuator type into the structural design – triggered both, system-wise as well as structural-wise. So tests have been performed with regard to both aspects, and although this was not planned beforehand, the demonstrator includes the original actuators and it also includes more structural elements in cordwise direction than originally planned. The concept has been tested by a set of tests. Test articles have been manufactured by the partners. The tests include many flat CFRP plates with a set of three aligned slits. The size of these specimens ranged from wide coupon tests to plates with a dimension of approximately 750 x 750 mm^2. Static and fatigue tests have been performed under a range of loading conditions. This includes tension in a direction perpendicular to the aligned slits as well as under 45° and under shear loading. A very high remote strain state has been used in these tests to challenge the disturbed plate design. Even at this high strain the performance was quite satisfying. As a kind of final verification a demonstrator – as mentioned above – with 2 m span has been tested under static and cyclic fatigue loading. The type of loading was a combination of bending and torsion. Finally a mock-up demonstrator of a full-sized section of a flap has been manufactured and handed over to the WP leader of the Clean Sky project.

The partners involved in the project were:

- Institute of Aircraft Design and Lightweight Structures, TU Braunschweig (IFL)
- Institute of Aerospace Engineering, TU Dresden (ILR)
- Institute of Lightweight Engineering and Polymer Technology, TU Dresden (ILK)

In addition, from CleanSky consortium Airbus Group Innovations was heavily involved.

2. Summary description of project context and objectives

High lift devices are currently used at aircraft to ensure sufficient low speed performance during take-off and landing. The high lift system usually consists of slats at the wing tip and flaps at the wing trailing edge. These high lift devices are stiff structures that are movably mounted on support tracks. During take-off and landing they are deployed to improve lift and during cruise they are retracted to minimize drag. The flaps are usually built up with an outer skin, several spars that run in span wise direction and many ribs in flight (chord) direction.

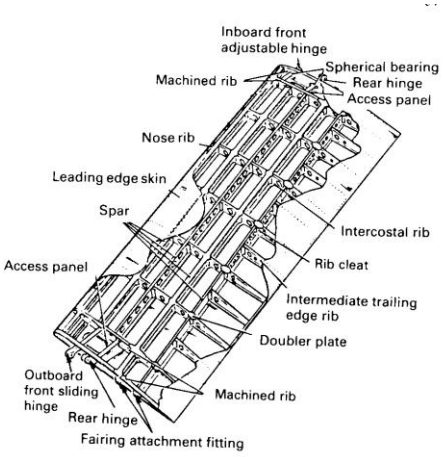

Figure 1: State of the Art Flap Design

The high lift performance of a state of the art aircraft is usually done by passively enriched boundary layers (single or double slotted flaps with fowler effect). Active flow control devices are seldom, but can be found at a few aircrafts (e.g. Antonov-72 and 74, Hunting H.126…) by using the jet stream from the engine to improve the high performance. This is achieved only locally in the region of the engines and not globally for the whole high lift system. The externally blown flap leads also to difficult design requirements regarding temperature stable materials for the high lift system.

Current high lift structural components are not designed to integrated active systems. Therefore the preferred FNG flap had to be redesigned in order to allow an integration of an active flow control system. This also includes the implementation of AFC outlet structures and new reinforcements to ensure the loading can be carried despite the large cut outs for the outlet structures. In addition, concepts had to be created for the integration of the AFC system containing, chambers, air pipes, outlet structures with actuators. For these devices, additional brackets, fittings and support structures had to be designed and integrated into the flap. To verify the design demonstrators of the preferred concept had to be built, which needed to be validated in a structural subcomponent test, see **Figure 2**.

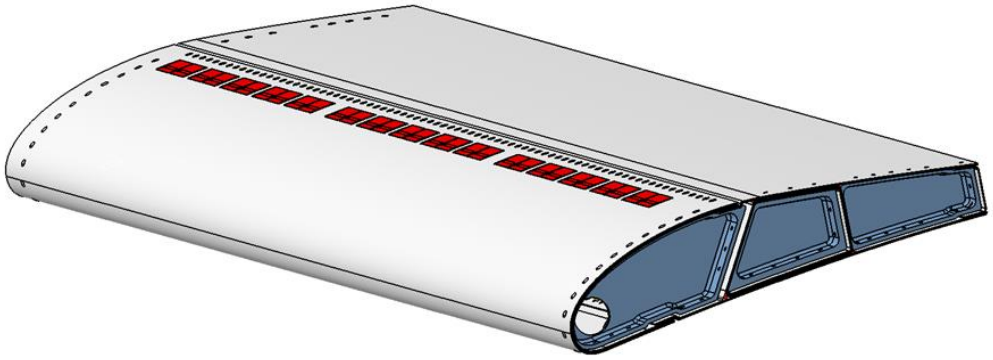

Figure 2: AFC Subcomponent Test Specimen

Many of the actuators currently under investigation for AFC systems are still existent in laboratory scale. In the present work the integration of a pulsed blowing fluidic actuator into a CFRP flap of a generic civil airplane is shown. To achieve airworthiness, the actuator is designed as a lightweight component. Due to the integration of the pressurized plenum in the flap leading edge structure a functionally integrated design in achieved, which requires no additional piping and adapters. Thus, the innovative design contributes to the weight saving.

…

3. Main S&T results

The project comprises several steps. Starting with the design concept, the sizing of the flap and the slits in the structure, tests of both, slit specimens and a flap specimen follow. In the end the mock-up demonstrator is shown. These parts are reflected in the following sub-chapters.

3.1 Design concepts (ILR, ILK and IFL)

In the first phase design concepts for the different project aspects had to be found and evaluated. The first step was the investigation of overall structural concepts. In a second step potential configurations of the outlet areas were examined. Finally a concept for the structural and functional integration of the outlet, delivered by the aerodynamics group of TU Berlin ILR [Bau12], had to be developed. The **AFCIN** project was heavily linked to the **FloCoSys** project due to the fact that it defined the type of actuator. This is the reason, why – from the very beginning of the project – common meetings and many telecons have been held and a close connection with both, Airbus and EADS-IW (now Airbus Group Innovation) has been maintained from the beginning. This contact was crucial also to define geometry as well as loads. Due to the very close interaction of the different partners, the entire task was characterized by the multidisciplinarity of the approach.

Requirements

The following requirements were specified by the partners and other subprojects or defined during the concept phase:

- General:
  - Air outlet at 20% chord at an angle of 45° with respect to the skin on top of the flap in downstream direction
  - Cruise conditions (-56°C)
  - Clearance (½ inch)
  - Maintainability
  - Structural solution shall be applied to the outboard area of the inboard flap
- Systems:
  - Accessibility to systems has to be assured for mounting and repair
  - Plenum surface area of ≈2830mm² or the equivalent surface of a pipe with 60mm inner diameter
  - Additional space requirements for control systems (valves, …)
  - 500mbar plenum differential pressure with respect to atmospheric pressure
- Actuator:
  - Tightness (actuator ↔ flap; actuator ↔ skin)
  - Possibility of actuator leakage test before integration into flap structure
  - Connection of at most five actuators among themselves in spanwise direction
  - Not load-bearing if possible
  - Keep deformations at a minimum
- Outlets:
  - Erosion protection has to be ensured in case of CFRP outlet solution
  - Tight connection to actuator
- Materials:
  - Avoidance of electrochemical corrosion
  - Thermal extension behavior in case of multi-material structures

Additional facts where observed but considered uncritical:

- Electrochemical corrosion:

  - Can be avoided by use of glass fiber layers on CFRP in case of CFRP – aluminum contact partners
- Air supply temperature
  - If bleed-air (max. 200°C) is used for plenum air supply it has to be ensured that its temperature is reduced to acceptable limits before entrance in the flap or CRFP-solutions with thermoset resins cannot be used

Furthermore it has to be made sure, that the natural frequency of the derived structural solution does not coincide with the actuator excitation frequency. This cannot be investigated until the structural concept is known.

Preliminary structural design concepts

Concepts

Despite more individual designs were developed in early design stages, only the main characteristics are presented here.

Differential designs

Differential designs are characterized by a large amount of separate components. It is conceivable to build the flap from separate spars, skin sections and other stiffening elements. This results in a high flexibility for the structural design and good maintainability but also increases the manufacturing and assembly effort and thus the costs. Various different differential designs are presented in Figure 3. The structure is shown in grey, the black box representing the actuator is shown in green, and a white box with black edges represents the space consumed by the systems and pipes. Connectors are shown in blue. All presented variations are based on a multi-rib design. Such concepts consist of a front and rear main spar, separate skin sections and numerous ribs in spanwise direction.

Design I As shown in Figure 3a, the actuator can be integrated in the main structure by connecting it to the upper skin with a number of partial ribs or rods along the span. The plenum and main systems can be integrated in the leading edge as well. The rear position of the main front spar can be seen as a problem. Furthermore, nothing is known about the mass of the actuator at the start of the work package. Therefore it cannot be secured, that the attachment of the actuator via ribs or rods is sufficient regarding flight loads. Additionally the assembly of such a structure is difficult regarding a proper connection to the outlets.

Design II This is an improvement of Design I. An additional actuator spar is established. The subunit of actuator and actuator spar can be pre-assembled and integrated in the leading edge. Additionally systems and the plenum can be attached to the actuator spar. By connecting upper and lower flap skin bending and shear loads are introduced into the actuator spar and thus the actuator. If such a concept is used, the susceptibility of the actuator to deformations has to be investigated.

Design III Since the outlets are positioned at a chord location where, from the structural point of view, normally the main front spar is located, it is possible to integrate the actuator in a milled main front spar. Thus no additional structure is needed for the mounting of the actuator. The main disadvantage of this concept is that the main spar deformations would act on the actuator as well and a proper functionality cannot be assured.

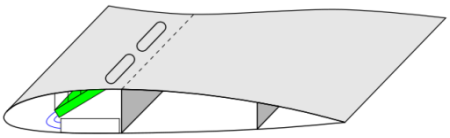

Figure 3a: Design I

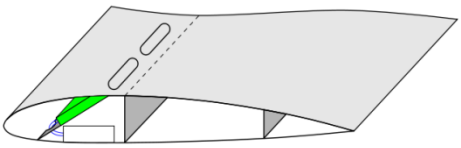

Figure 3b: Design II

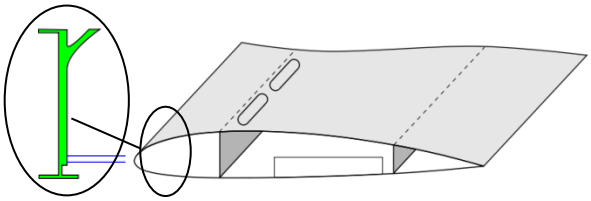

Figure 3c: Design III

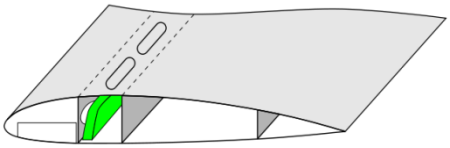

Figure 3d: Design IV

Figure 3: Differential designs

Design IV This design is the attempt to reduce the disadvantages of a front spar position behind 20% chord. An additional spar with web holes is used to support the main front spar. This spar has to be positioned as far away as possible from the flap nose. This results in a curvature of the actuator. According to information from the project DT-FA-AFC this is allowed in a limited amount. The main disadvantages of this design have to be seen in manufacturing and assembly efforts.

Integral designs

Instead of multi-rib designs the concepts shown in Figure 4 are based on a multi-spar design. Hence, they consist of an integrally manufactured combination of skin and frames. All integral designs are characterized by a high stiffness in spanwise direction. On the other side it is difficult to assure the accessibility to the actuator and the systems and the manufacturing itself is very expensive. All multi-spar concepts additionally share the problem of proper rib integration. It should be paid attention to this problem since at least one rib will be needed in the FNG inboard flap.

Design V This design is based on the idea to locate actuator and systems in one compartment between two spars. The actuator is mounted as in Figure 3a or supported by a spar. Despite the apparent advantages of such a design the manufacturing will be very difficult. Furthermore as in differential design I it cannot be assured that such a mounting is applicable. Additionally the assurance of proper system accessibility decreases the advantages resulting from this design.

Design VI This is a slight modification of concept shown in Figure 3a. It can be seen in Figure 4b in which actuator and systems are located in two different compartments. So, the decrease in stiffness at the actuator location is reduced compared to concept V. Nevertheless, the design suffers from the same disadvantages.

Geodesic design

[Uri08] presents another structural design approach. In the paper two integral designs for future small aircraft are presented that can also be used as flap designs. The introduced geodesic design uses two main spars and a skin made of tapes and a thin sheet. It is illustrated in Figure 5.

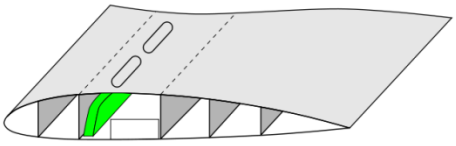

Figure 4a: Design V

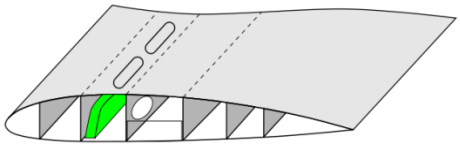

Figure 4b: Design VI

Figure 4: Integral designs

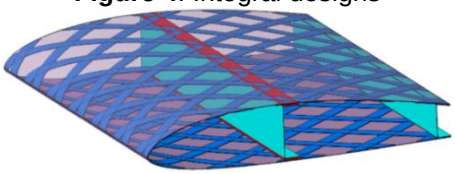

Figure 5: Geodesic design **[Uri08]**

For application of the design in the flap with an AFC-system the tapes could be positioned to allow the presence of thin sheets at the outlets. Since those thin sheets would not be regarded as structurally significant and load-bearing the outlets would not be a structural impairment.

Nevertheless the manufacturing of the structure and the assembly and actuator integration have to be assessed as difficult and expensive. Furthermore maintenance and repair efforts would result in the manufacturing of a new flap.

Multi-web box design

Another approach presented in [Uri08] is a multi-web box design as shown in Figure 6.

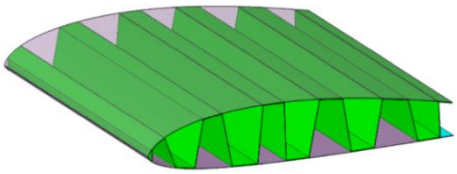

Figure 6: Multi-web box design **[Uri08]**

It consists of an integrally manufactured web profile and a separate skin. Like multi-spar designs it provides a high stiffness in spanwise direction. For the integration of AFC-systems and actuator the skin has to be divided. So the actuator and AFC-systems can be pre-assembled on a bearer and integrated in a compartment between two webs. In addition to the difficult manufacturing of the multi-web structure the space in a compartment between two webs is limited to ensure a sufficient stiffness. A further investigation of this concept is therefore excluded due to the high required space of the plenum and additional systems.

Conclusion

None of the presented designs fulfills all requirements. While differential designs lack the necessary stiffness, the purely integral multi-spar solutions are not applicable because of the accessibility constraint. Based on the evaluation of the requirements and the concepts it is found that a flap with a differential leading edge, integral main box and arbitrary trailing edge combines the advantages of differential and integral designs and is therefore the preferred solution. A cross section of a possible structural design can be seen in Figure 7.

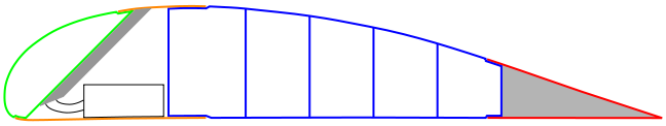

Figure 7: Mixed Design

AFC integration concepts

Concepts for the integration of the actuator, plenum and other systems into the flap structure had to be developed based on the structural design concept or the other way around. If an integral main flap chamber is used (see Figure 7) on the condition of the outlet requirements defined in section 0, the AFC-system can only be integrated into the leading edge.

ZI-spar-actuator

This is a concept motivated by assembly and maintenance considerations. The spar has two functions. The spar integrates a structural and an actuator function. At first it realizes the leading edge stiffness and is secondly part of the actuator. The concept is shown in Figure 1. Gaps for AFC and holes for the connection to the leading edge will be milled and drilled in the leading edge skin. The actuator consists of two parts, the Al actuator and the base plate (spar). The actuator is a machined aluminum block and includes the actuator shape. Both parts, actuator and base plate, are able to connected and tested separately. Then the plenum can be attached. The leak tightness of all parts of the AFC-system can be checked separately in a lab. The system will be inserted into CFRP leading edge. Tolerances will be managed by floating rivet nuts and insert holes (hand drawing red).Adjustment of both structures will be realized by insert-adapter and screwing together. The complete installed leading edge will be riveted to the main flap structure. The actuator is able to carry loads, but the influence of actuator deformation of the AFC cannot be estimated.

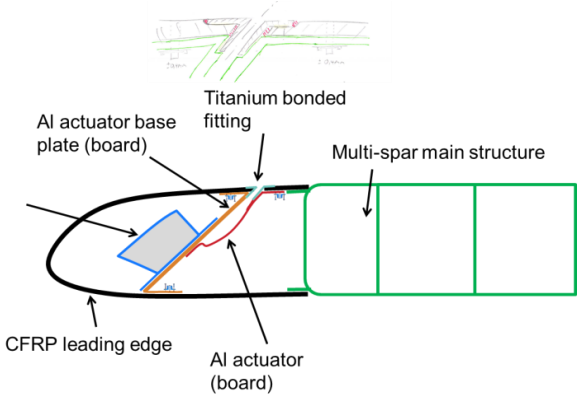

Figure 8: ZI-spar-actuator concept

C-spar-actuator

The C-spar-actuator concept is mainly driven by applying as much as possible FRP-parts considering a cost-efficient production. Furthermore it was focused to divide the outer skin into as few as possible parts. The name C-spar-actuator results from the C-shaped cross section of the front spar. The basic design is shown in Figure 9. Several concepts concerning the partition of the outer skin have been developed and compared considering stiffness, manufacturing as well as accessibility of the actuators for maintenance. Two exemplary C-spar-concepts with different partition of the outer skin are shown in Figure 10. Both concepts exhibit a closed middle section without any openings in the outer skin which is advantageous under torsional loading. The openings of the actuators are located within the

outer skin of the leading edge. Concept 2 allows a full access to the actuators by dismounting the leading edge (skin panel 3) whereas the accessibility of the actuators is limited in concept 1. Furthermore the skin panel 2 in concept 1 has an undercut. Due to these comparison concept 2 was chosen as a favourite C-spar-actuator concept.

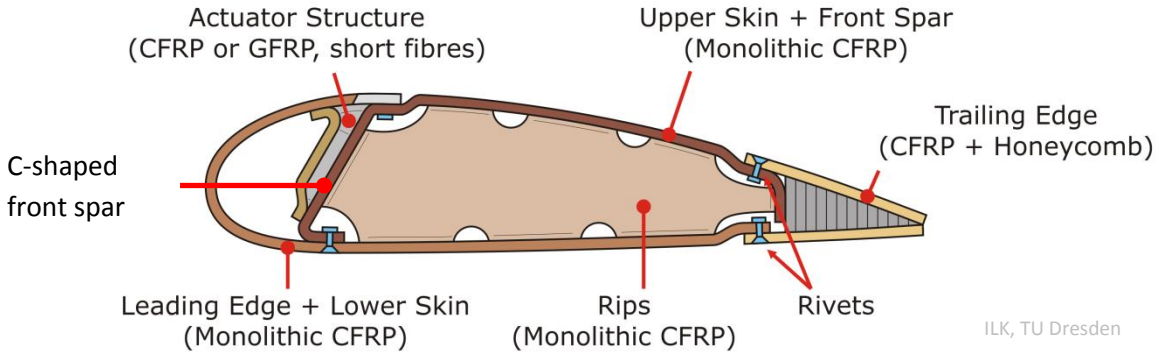

Figure 9: C-spar-actuator concept

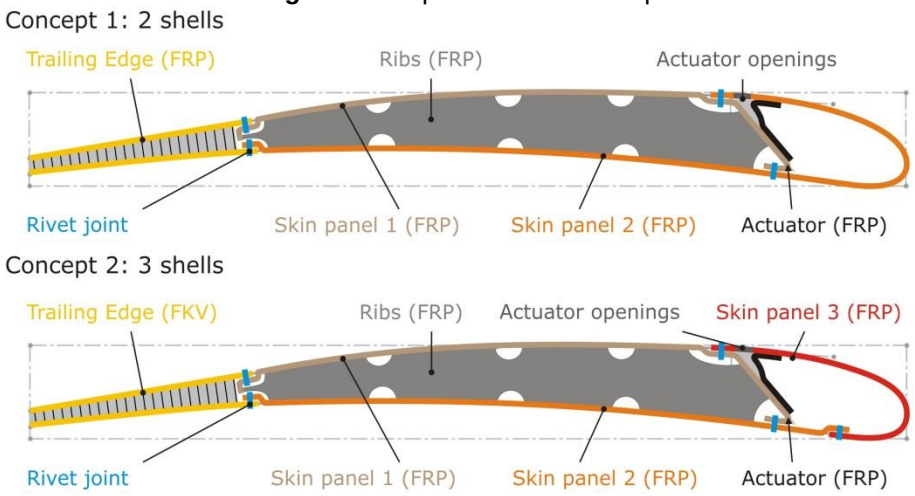

Figure 10: Comparison of C-spar-concepts

A more detailed model has been created for concept 2, which is shown in Figure 11. The actuator shell can be manufactured by autoclave, vacuum assisted resin infusion or injection moulding. However the actuator shell is deformed under bending or torsional loading of the flap due to the permanent joining to the load-carrying front spar.

Y-spar-actuator

This is a concept motivated by assembly considerations. It relies on the assumption that it is possible to build a non-load-bearing leading edge. Therefore, the torsional loads have to be carried by other structural members. An additional slanted front spar is introduced. Since loads resulting from the pressure distribution along the chord are currently unknown no information can be given which loads the leading edge has to withstand anyway. The basic ideas of this concept are shown in Figure 12. A split actuator is proposed with a rear wall acting as mounting base for integration of brackets also. Those can be used to retain plenum and systems.

ZI-metal-spar-actuator

Because of the potential erosion risk, a CFRP-solution for the outlets would always require metallic inserts. Since the effects of holes in the CFRP-plates combined with fatigue loading and erosion are not fully known, the metallic solution is expanded to the whole outlet module in this concept. Figure 13 shows the basic ide

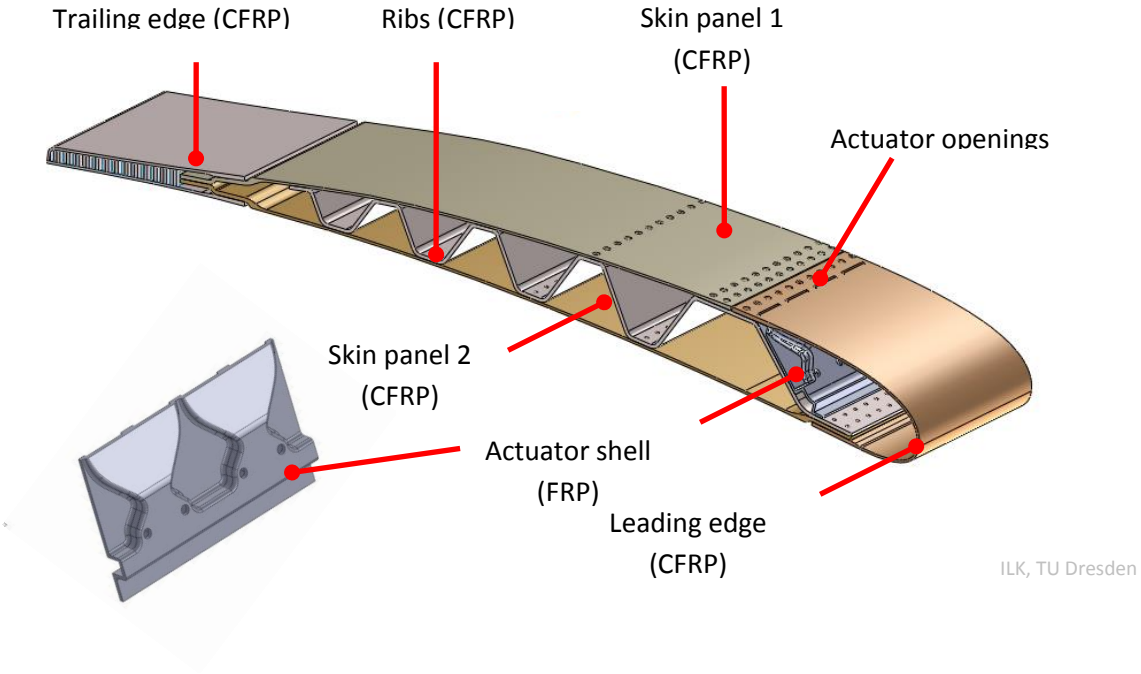

Figure 11: Detailed design of concept 2 (C-spar-actuator)

This concept presumes a load-bearing leading edge and an integral main flap box. The latter is assumed to create the necessary bending stiffness. Therefore, torsional loads are acting on the leading edge. The load transmission is realized via the outlet module. It consists of two flanges, the outlet openings and internal ducts which reproduce the upper part of the actuator geometry defined in [Bau12]. The actuator rear wall is attached to the outlet module. It also acts as mounting plate for plenum and systems. At the top it is milled to house the outlet module and thus assure the reproduction of the actuator geometry. The tightness can be realized with a gasket. Mounted on the actuator rear wall is the actuator profile with a similar connection to the outlet module.

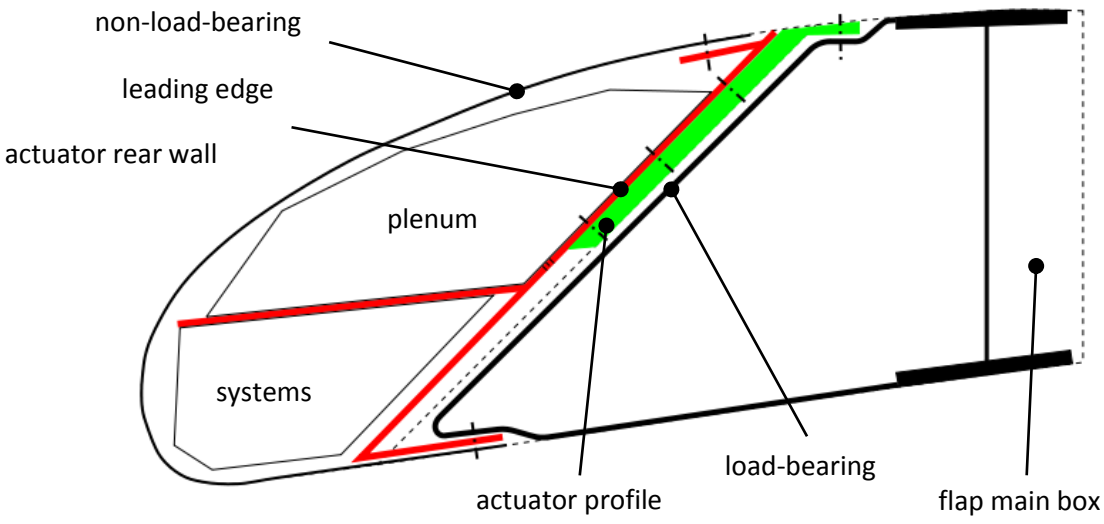

Figure 12: Y-actuator concept

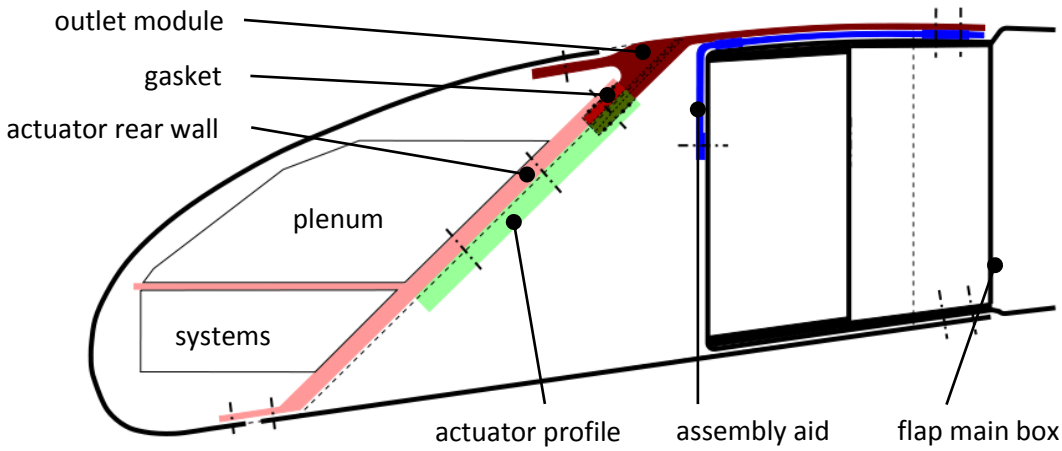

Figure 13: ZI-metal-spar-actuator concept

The leading edge is mounted on the outlet module and the actuator rear wall. An assembly aid is used to ease mounting of the structure to the flap main box. This way it is possible to place the fasteners to a rearmost position. Thus they are not affixed in the area of highest bending loads. After an extensive analysis by all partners, it has been decided to use the ZI-spar version.

3.2 Sizing of the flap and the flap test specimen (ILR)

3.2.1 Sizing of the flap

To identify the structural performance of the FNG-AFC-70 a detailed FE-model (**Figure 14**) for a CFRP multi spar inboard flap was built up. This FNG-AFC flap was attached to a 1D stick model which bases on previous industrial investigations. Integrating this stick model enables a consideration of defined failure load cases e.g. free wheel, which are locally dimensioning for the flap. Furthermore the surrounding attachment stiffness reproduces and ensures realistic boundary conditions.

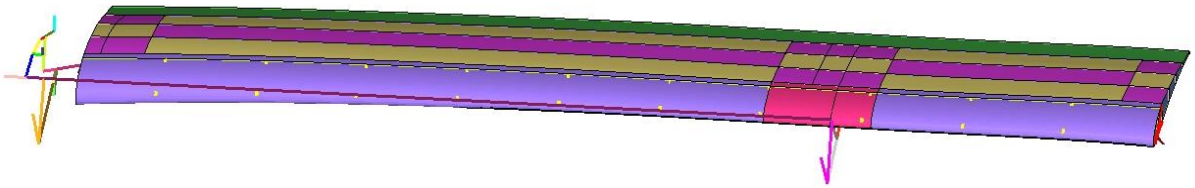

Figure 14: Static FE-model for FNG-AFC-70 flap

From industrial side relevant load cases were defined. Since the passive FNG is 25 % larger in span and chord direction the FNG loads are estimated 1.56 times larger compared to the loads given from industry. 7 sizing load cases were considered. Also the provided air load data needed to be scaled. The normal and transverse loads were determined making a calculation of FNG flap which is only fixed by a single fixation (SPC – single point constraint) point. These loads (0°-cruise, 15°-T/O and 50°-landing) were scaled for each load case. Hence the used loads base on FNG air load which are scaled basing on industrial input.

The load cases include:

- LC01 as a normal loadcase at V_f and 40 degree; where strength and buckling are expected to be essential

- LC04 as a further normal loadcase a V_D and 2.5g with airloads and wing bending; again strength expected to be of sizing nature
- LC05 as a failure case
- LC08 an other failure case
- LC10, LC11 and LC12 as cases, where torsional, bending and again bending stiffness is expected to be essential

Basing on experience from previous projects the stiffness of the flap is next to stability and strength a dimensioning criterion. **Figure 15** shows the gap criterion in extracted position of the flap. The deformation of the flap is measured during the optimization process on defined spanwise positions. This approach is used for landing (LC12) and T/O (LC11) configuration. The allowable displacement of the flap was defined by Airbus.

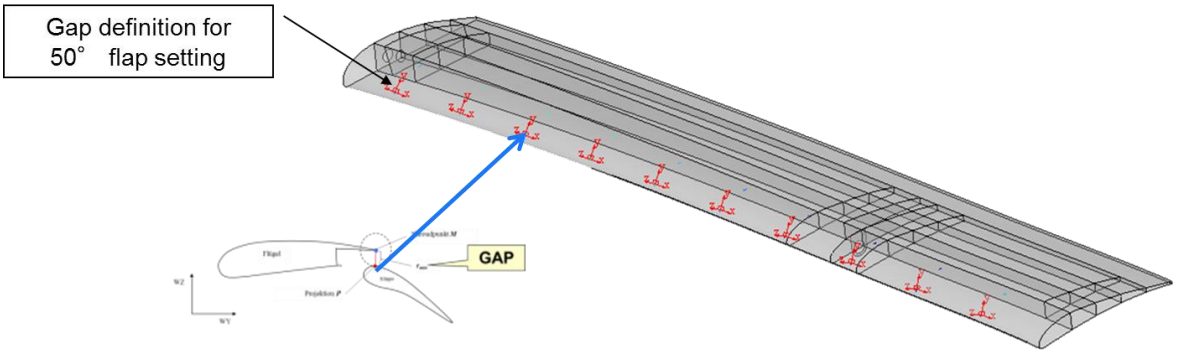

Figure 15: Stiffness measuring in extracted position

Next to the stiffness, several strength, strain and stability constraints were defined for the optimization process. These constraints are considered within LC 01, 04, 05, 08 whereby load case ID 01 is the most dimensioning flight attitude. The size optimization using Optistruct considers defined design variables. This means that e.g. the laminate stacking of a pre-defined area is automatically adapted by the optimizer to a configuration fulfilling the defined constraints. Each color of the flap in **Figure 14** symbolizes such a separate sized area. All together the model has 216 design variables whereby 1 design variable belongs to 1 ply or for the metallic ribs to one rib. Furthermore manufacturing and stacking rules are considered within the optimization e.g. to have balanced lay-up.

15 iteration steps were necessary to get a feasible flap design considering all defined constraints. **Figure 16** shows the composite failure index for strength critical LC01. Within the area of track 2 the reserve factors of FNG-AFC-70 flap are close to 1. Thicknesses of the area between track 1 and 2 are sized by stiffness constraint. This can be reasoned since the allowable displacement of the flap is exactly met but strain, strength and stability is not critical for this area. **Figure 17** shows the first eigenvalue of 1.27 of the AFC-flap. Stability of the flap is not a significant dimensioning constraint. For that, in course of the sizing process, buckling was only considered for the most critical load case LC01.

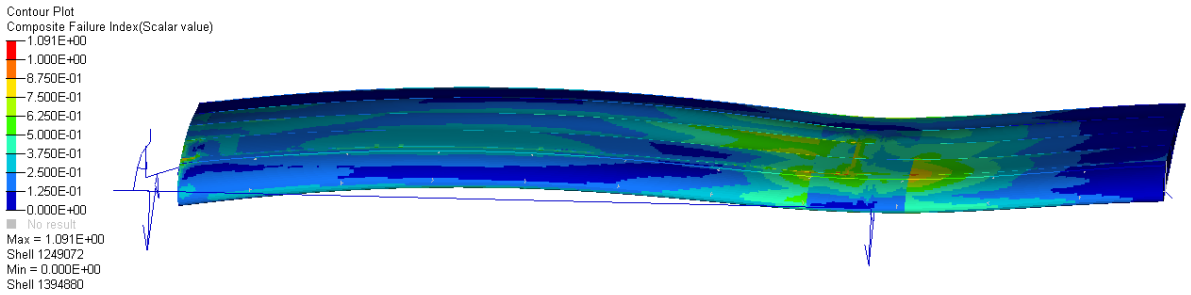

Figure 16: Strength plot for dimensioning load case LC01 – Normal case V_D 50° flap setting

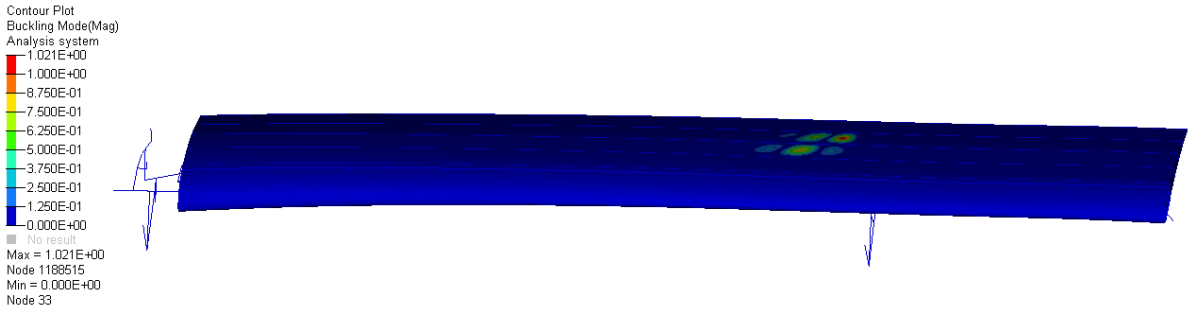

Figure 17: First buckling eigenvalue 1.27 for LC01

Basing on the defined design variables and belonging areas **Figure 18** shows the resulting thickness plot. It must be mentioned that the thicknesses of the LE at track 2 is not feasible. This is caused by some singularities from load introduction. The thick upper skin and leading edge area between track 1 and 2 is mostly dimensioned by the stiffness constraint. Basing on the LE thickness the laminate stacking sequence for plate test with slots for AFC system were defined.

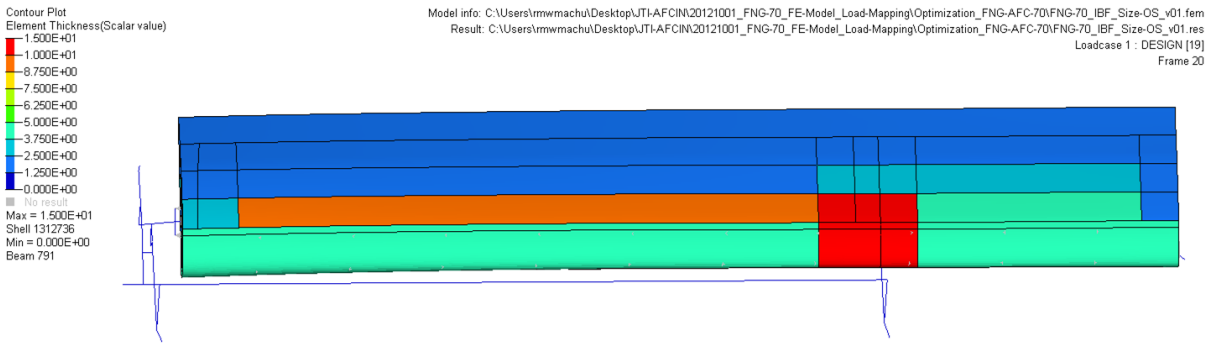

Figure 18: Thickness distribution of sized FNG flap

Extrapolating the weight of an A320 inboard flap (25 % larger in chord and span) the passive FNG100 flap would have a weight of around 90 kg. To verify this weight currently a FNG100 model is built up and will be analyzed. Compared to the passive flap the smaller AFC-flap has a weight of around 70 kg.

3.2.2 Sizing of the flap test specimen

In preparation for the full-scale flap static and fatigue test a finite element model was created to determine the limit loads. Based on the optimization results a full-scale static and fatigue test specimen was built at EADS Innovation Works (now Airbus Group Innovation). It was planned to include many more cells in cordwise direction than foreseen in the Work Description. Due to

manufacturing problems the test specimen planned was not built in that very extended way. It was decided to shorten the specimen in chord-direction. Thus, only one core is necessary in the production of the structure. But this still means a much larger specimen than planned in the Work Description. The big advantage is that this fits testing requirements much better. Except for the open rear box, the geometry of the new test specimen is identical to the previous structure. The CsCalc model for the calculation of the shear center can be seen in **Figure 19**.

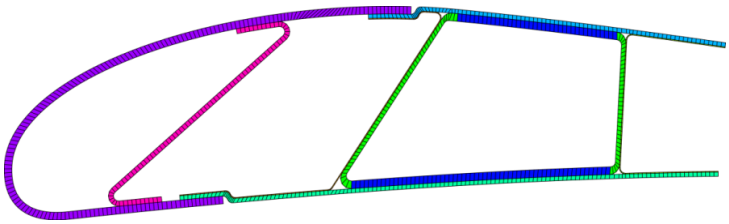

Figure 19: Demonstrator CsCalc model

The specimen is reinforced in the outer and middle cross-section for the bearing and load introduction. The bearing is represented in the finite element model by stiffening the complete cross-section. The aluminum reinforcement necessary for the load introduction is modeled based on different property sets for the shell model as shown in **Figure 20**. The width of the load introduction collet is changed to 70mm in the new model.

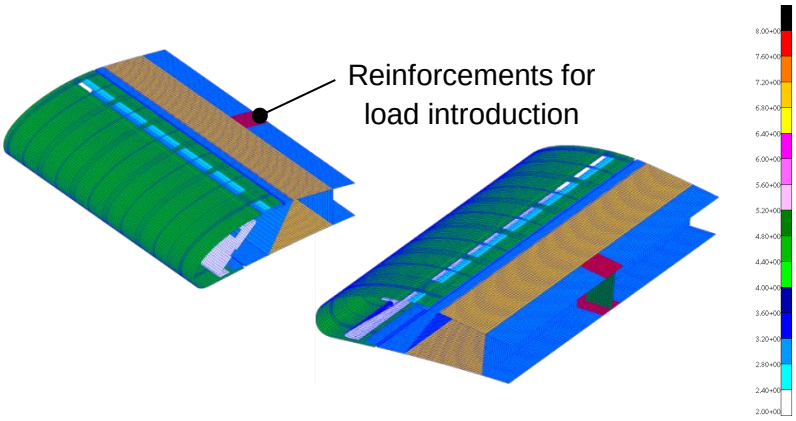

Figure 20: New model: load introduction reinforcements, thickness plot

Table 1: HTS40/RTM6 ply material data for ϕ_F=55%

Type	Description	Value	Unit	Type	Description	Value	Unit
Stiffness	E_1	133	GPa	Failure	R_1^T	1500	MPa
	E_2	7.5	GPa		R_1^C	750	MPa
	ν_{12}	0.3			R_2^T	70	MPa
	G_{12}	3.8	GPa		R_2^C	220	MPa
					R_{12}	55	MPa

The test specimen uses the HTS/RTM6 carbon fiber/epoxy composite defined in **Table 1**. Standard aluminum 2024 from HSB 12512-01 is used for the modelling of the load introduction reinforcement of the rear skin. The reinforcement thickness is taken from the specimen CAD-model.

The inner and outer cross-sections of the test specimen are stiffened by thick aluminum ribs, assembled in the leading edge and the main box spar. Thus, it is legitimate to assume that these cross-sections are stiff enough to be assumed as rigid. To model the bearing, the nodes of the inner and outer cross-sections, respectively, are connected to a central node positioned in the cross-section shear center by a rigid RBE2-element as shown in **Figure 21**.

Several first-ply-failure and progressive failure criteria are implemented in PATRAN for use in the post-processing of a finite element analysis. For the model used in this analysis, these are not applicable since PATRAN aborts the layer-wise failure analysis due to a programming error. Despite several attempts to solve or circumvent the problem a first-ply-failure analysis was not successful for the used models. Thus, the commonly used maximum strain criterion is applied to determine the flap limit loads. The maximum tension (positive) and minimum compression (negative) strains are determined over all laminate layers. Based on values provided by EADS Innovation Works, maximum tension strain is 4000µstrain or 4.0‰ and the minimum compression strain is -3500µstrain or -3.5‰. The evaluation is performed for all elements outside the bearing influence zone.

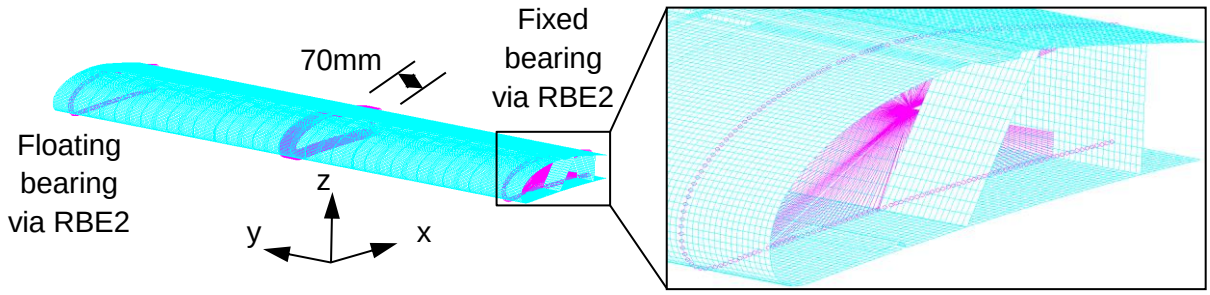

Figure 21: boundary condition modelling

At first, the static bending load case was simulated. The deformation meets the expectations, based on the simply supported and clamped boundary conditions. In the area of the highest deformation it can be seen, that the deflection on the trailing edge is higher than the one on the leading edge. This is expected, due to the varying shear center in each flap cross-section. It is obvious, that a combined bending-torsion load case is acting. The limit load with a reserve factor of one for the maximum principal strain criterion is -73969.3N. The z-displacement maximum is 12.2mm in negative z-direction and therefore is in a meaningful range. The y-displacement in the floating bearing is sufficiently small with -0.24mm. A maximum principal strain of 4‰ is achieved on the lower side of the skin at limit load (F_z=-73.9kN) as expected. The plot of the maximum principal strain distribution is shown in **Figure 22**. The strain maximum occurs at the border of the stiffened collet load introduction area and the adjacent skin near the trailing edge. This area is stiffened by the aluminium rib shown in **Figure 20**.

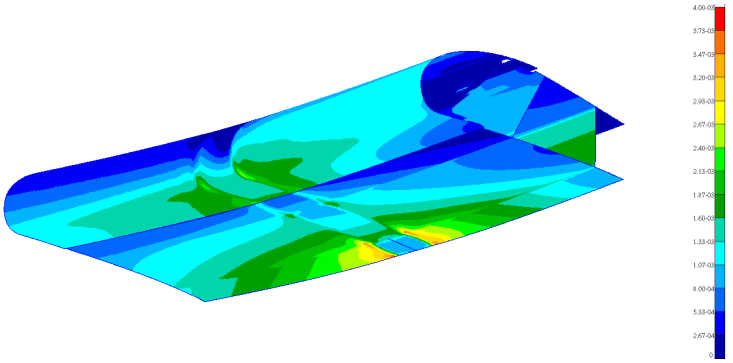

Figure 22: bending, maximum principal strains at limit load (F_z=-73.9kN)

The minimum principal and thus compressive strain is present on the upper skin, in the area between the box spar and the connection to the differential leading edge. A minimum strain of -3.4‰ is achieved at limit load (F_z=-73.9kN). The strain distribution can be seen in **Figure 23**. In order to eliminate the risk of stability problems during the fatigue test, a linearized pre-buckling analysis was performed for the bending load case at the limit load of F_z=-73.9kN with the same boundary conditions as for the static test. The critical eigenvalue is 1.505. Therefore, buckling is uncritical. For the reversed load direction, in case the flap is mounted in the test rig due to measurement reasons, the first eigenvalue is 1.451 and thus uncritical as well.

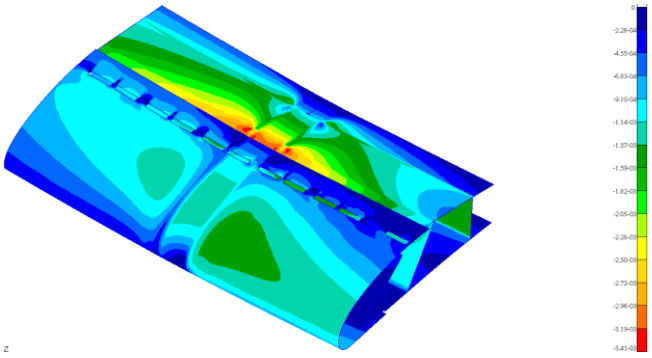

Figure 23: bending, minimum principal strains at limit load (F_z=-73.9kN)

Similar results are found under torsional loading.

3.3 Sizing of the slits and the slit test specimens (ILR and ILK)

In order to justify the sizing of the skin of the flap in the vicinity of the slits several actions have been taken. This includes both intensive calculations and testing.

3.3.1 Sizing of the slit surrounding structure

Finite elements calculations were performed with the software package PATRAN/NASTRAN to obtain the loads for the fatigue tests. Static and fatigue tests of the leading edge structure around the outlets of the active flow control (AFC) system are carried out, to evaluate the structural behaviour of this region. The slightly simply curved region of the leading edge is represented by slotted flat plate specimens. Two separate plate types were produced, which contain the different coupon test specimens. The two plates and the respective specimens can be seen in **Figure 24** and **Figure 25**. Plate type one is manufactured three times while only one plate of type two is necessary such that three specimens of each type can be tested. The plates for fatigue testing are marked in the figures.

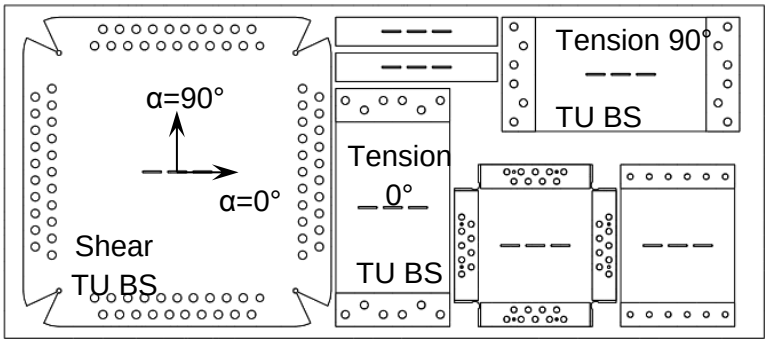

Figure 24: Plate type 1

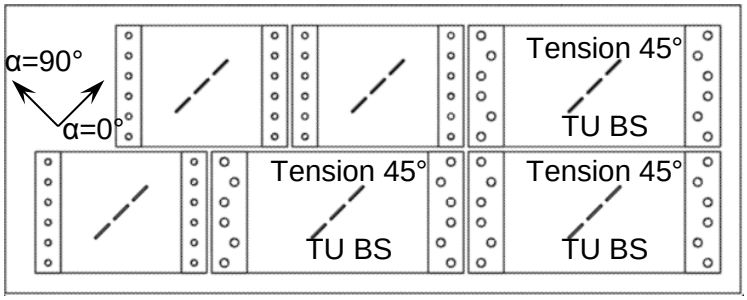

Figure 25: Plate type 2

The material 0° degree direction is aligned with the slots. The original configuration of the flap leading edge is shown in **Figure 26**. The two outlets of one actuator have a distance of 13mm and two adjacent actuator outlets are 26mm away from each other.

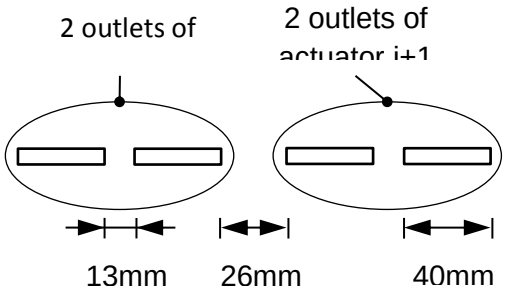

(a) outlet dimensions (1)

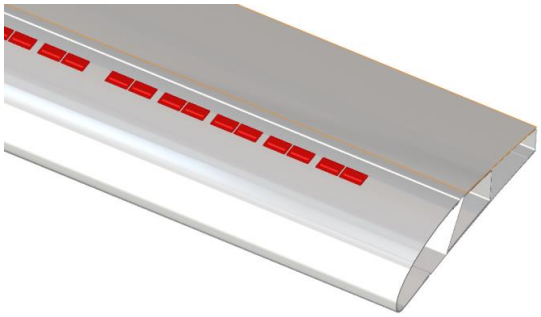

(b) outlets with inserts from demonstrator model

Figure 26: Outlet geometry

Due to limitations of the test fixtures, it is not possible two test specimens with these four outlet slits. The test rig is simply not wide enough to install the wider specimens and simultaneously provide the necessary load for the static tests until failure. On the other hand, using only the two slits of one actuator would not represent the possible interaction of neighboring holes. Therefore, the AFCIN project partners decided to use three slots with a constant distance of 13mm instead as shown in **Figure 27**. Thus, a conservative representation of the actual leading edge structure is provided.

During the manufacturing of the static shear specimen an error occurred. Since a new plate had to be prepared it was decided to manufacture another hole configuration with only two slots and 26mm distance. Two plates of the two configurations were tested.

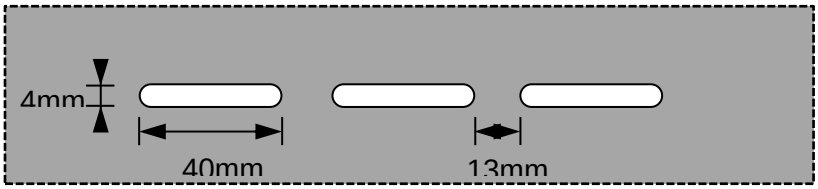

Figure 27: Coupon test plate outlet geometry

Finite-element models of all tension tests (0°, 45°, 90°) as well as the shear test (0°) have been created using two dimensional shell elements for the coupon plates (Abaqus element type: S4). The element size around the holes was chosen very small to get more realistic results in this area (see **Figure 28**). The material data used are listed within **Table 1**.

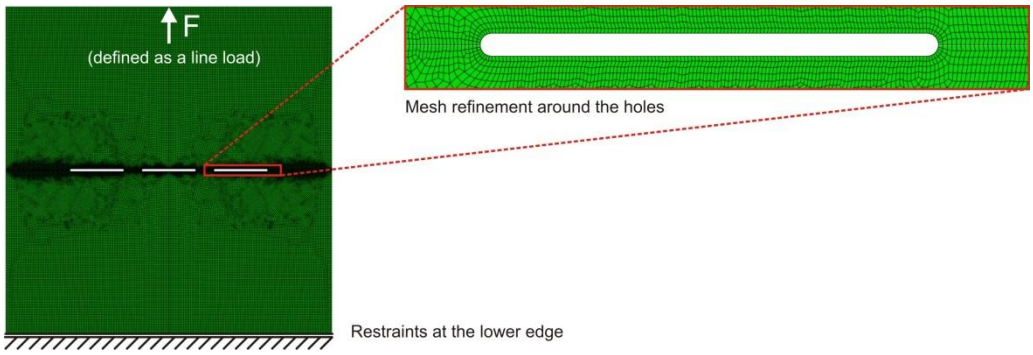

Figure 28: FE-model of the tension test 0°

Figure 29 exemplarily shows the simulation results for the shear test (0°). A linear eigenvalue analysis has been carried out at first to determine the buckling load of the coupon, which is about 80 kN for this example. It has to be mentioned, that imperfections were not considered within this preliminary analysis. In a second step, the failure load of the coupon due to reaching the material strengths is determined. The physically based failure criterion according to Cuntze is used to assess the material effort within the single layers of the laminate. The resultant material effort according to Cuntze reaches a value of 1 at a force of 10 kN at the outlet corners in the example shown below. Thus, the buckling load is much higher compared to the failure load. So the down scaled laminate layup assigned to the coupons within this simulation is basically suited for the tests.

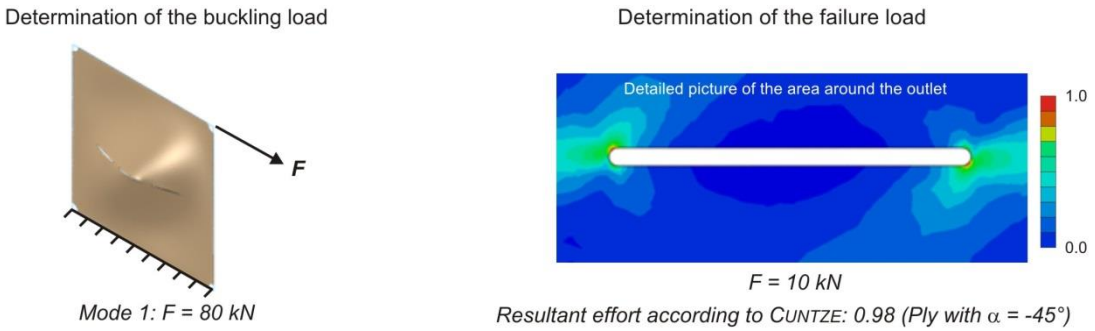

Figure 29: Exemplary results for determination of buckling load and failure load (shear)

3.3.2 Further, more detailed investigations

In a first step during this project several levels for the determination of stresses are developed or applied to the given problem. These are closed-form analytical solutions for the stress distribution around the contour of an arbitrarily shaped hole, the static finite element solution already used in section above and the XFEM-method for the implicit numerical simulation of the damage initiation and propagation in the outlets.

A parametric Python-script is used for the generation of the coupon models. This way, a fast, reliable method for the model generation is used. The script makes use of symmetry conditions. A graphical user interface is implemented to allow an easy input of data. The resulting mesh around the holes and the input deck in the graphical user interface are shown in **Figure 30**.

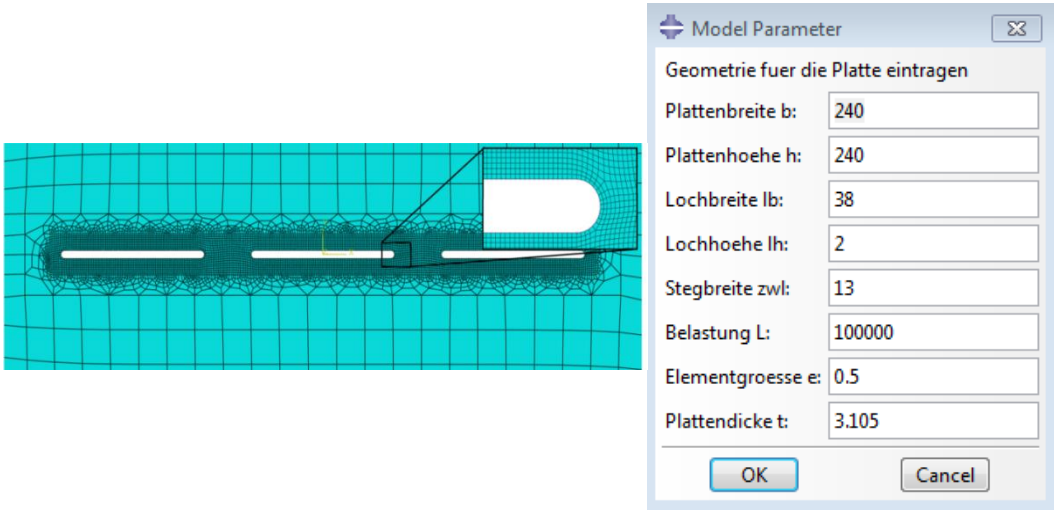

Figure 30: Mesh around holes in Abaqus and graphical user interface

The results of the static coupon tests are compared to the XFEM simulations. The optical, non-contact and material independent measuring system ARAMIS by GOM mbH is used during the test for the measurement of displacements and recalculation of strains in the test specimens. To validate the measurements and the XFEM simulations an evaluation of displacements of selected point around the outlet is performed. The chosen points lie on the hole contour an two close to the hole in the CFRP material. The point locations can be seen in **Figure 31**. The origin is in the center of the hole.

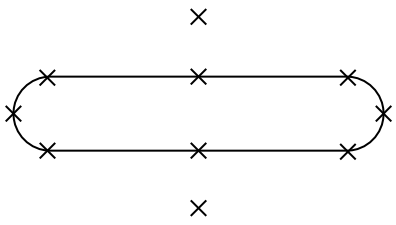

Figure 31: ARAMIS data evaluation points

The results of the displacement comparison are shown in **Table 2** exemplary for the 0° tension specimen at 62kN. The concordance of results is good. As expected, the 2D smeared modeling

approach shows a better agreement than for the generic model due to the coupon laminate build-up.

Table 2: Displacement comparison between ARAMIS results and simulation, 0° tension, 62kN

	2D stacked			2D smeared		
Point (x/y)	Test [mm]	Simulation [mm]	Δ [%]	Test [mm]	Simulation [mm]	Δ [%]
7 (0/-5)	0,402	0,385	4,23	0,402	0,387	3,73
2 (0/5,5)	0,168	0,157	6,55	0,168	0,161	4,17
6 (-27/-5)	0,305	0,304	0,33	0,305	0,316	0,34
4 (-27/0)	0,282	0,270	0,43	0,282	0,279	1,06
1 (-27/5)	0,259	0,232	10,42	0,259	0,240	7,34

The simulation calculates smaller deformations. Thus the model has a higher stiffness than the coupons. This can be caused by manufacturing imperfections or thickness variations of the coupon test plate. Similar behavior can be observed for the other coupons as well.

Generally it is difficult to obtain the correct failure loads from the ARAMIS results. The problem is shown in **Figure 32**. The gray value pattern is used for the ARAMIS measurement. Thus, ARAMIS can only measure values where such a pattern is present. This makes the evaluation of the hole contour very difficult. The problem is increased since the pattern is lost due to blistering in case of failure. This can be seen in the right subfigure of **Figure 32**. It is assumed that failure occurs as soon as the pattern is flaking off.

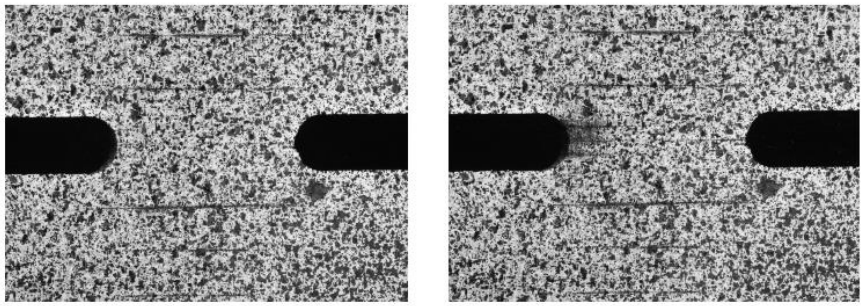

Figure 32: Comparison of undamaged and damaged specimen in the 0° tension test

The results for the 0° and 45° tension and the shear specimen are provided in **Table 3**. The 90° tension tests are not performed.

Table 3: Results coupon tests and XFEM simulation

	0° tension [kN]	45° tension [kN]	Shear [kN]
Coupons	82.5	80.0	76.0
2D stacked	77.2	85.4	117.0
2D smeared	59.2	77.9	76.9

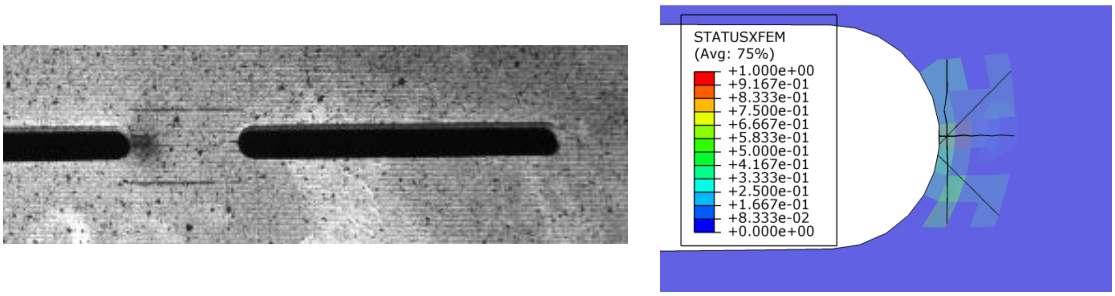

Figure 33: Damage location in coupons and XFEM for 0° tension specimen

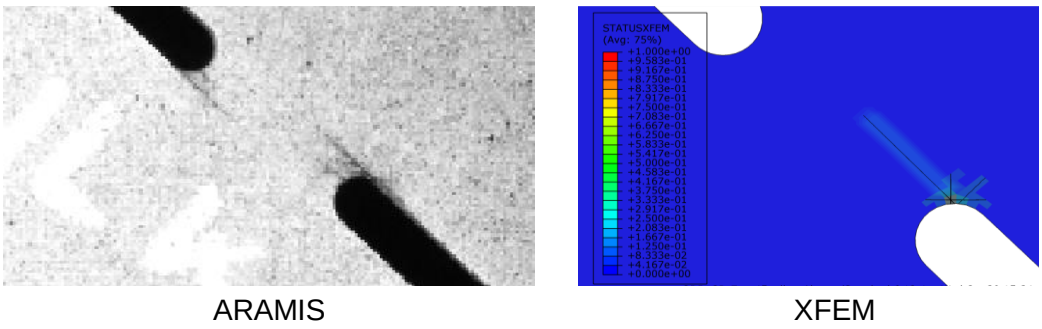

Figure 34: Damage location in coupons and XFEM for 45° tension specimen

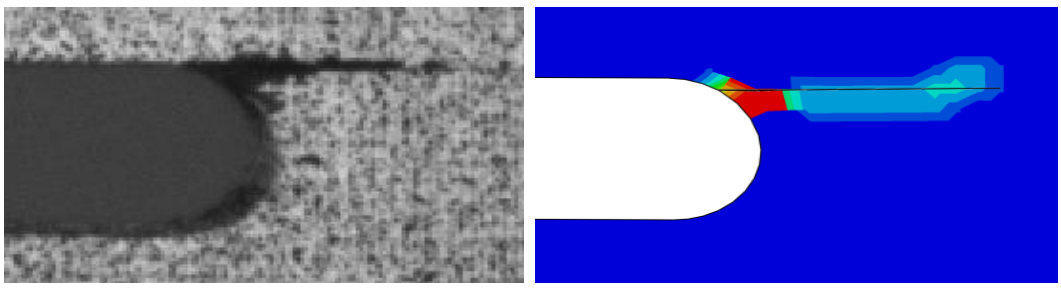

Figure 35: Damage location in coupons and XFEM for shear specimen

It can be seen that the 2D stacked models are able to predict the damage initiation for the 0° and 45° tension specimen. For the shear test the load is overestimated. For the shear specimen and the 45° tension test the 2D smeared stiffness approach delivers more adequate results. The use of the XFEM for CFRP materials shows the current method limitation. The 3D modelling promises better results. These have to be investigated in a future project with a high performance computer and more Abaqus license token available. The positions were failure occurs can be predicted pretty well. The damage locations for the three coupon specimens from **Table 3** are shown in **Figure 33**, **Figure 34** and **Figure 35**.

3.4 Flat specimen tests

3.4.1 Static tests (ILK + ILR)

The influence of the holes at the outlets on the mechanical behavior of the load-carrying CFRP-structure was determined by coupon tests. Therefore CFRP-coupons with holes similar to the outlet structure of the flap were tested under tension loads. The deformation of the CFRP-coupons especially around the holes was measured by grey scale analysis ARAMIS during the tension tests, which allows an optical determination of strains and displacements.

Figure 37 gives an overview of the different test rigs used for tension-tests 0°, tension-tests 45°/90° and the shear test. Here, three different clamping tools were used depending on the coupon size and loading. The slight coupons for tension 0° were clamped within an existing tool, whereas the coupons for tension 45° and 90° were clamped into the own developed test. The shear tests have been made using an existing clamping device of the ILR, TU Dresden.

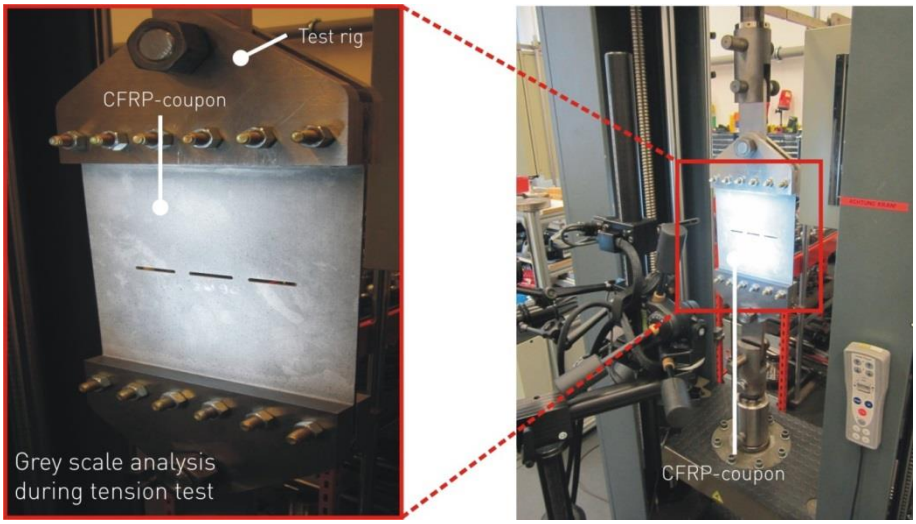

Figure 36: Tension test and grey scale analysis

Figure 38 exemplarily shows the experimentally determined strain ε_y in direction of the tension force compared to the strain ε_y of the FE-calculations. The results nearly show no difference. The notch effect of the holes and the resulting high strains ε_y between the holes are typical for this kind of coupon geometry. Furthermore the influence of boundary effects on the test results seems to be very small.

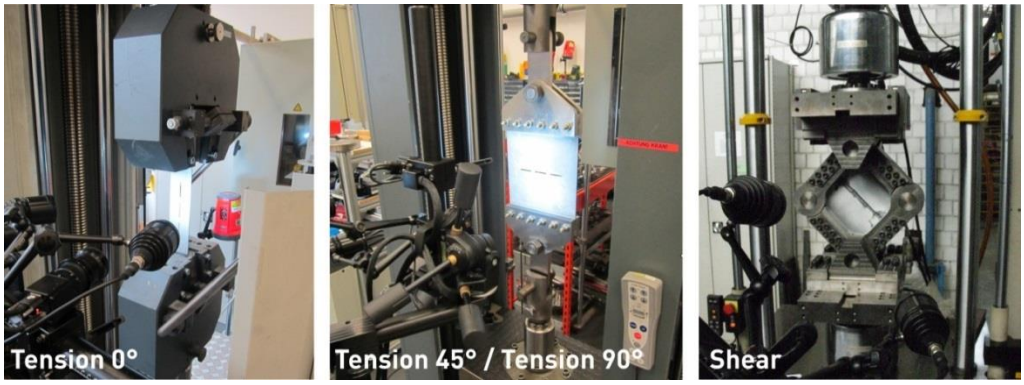

Figure 37: Test rigs for static coupon tests

The experimentally determined mechanical behaviour of the coupons under tension loading in three different directions has been used for sub-models in the FE-calculations carried out by ILR and EADS-IW. Furthermore the accordance of the results between FE-calculation and experiment in all tests approved the assumed material properties.

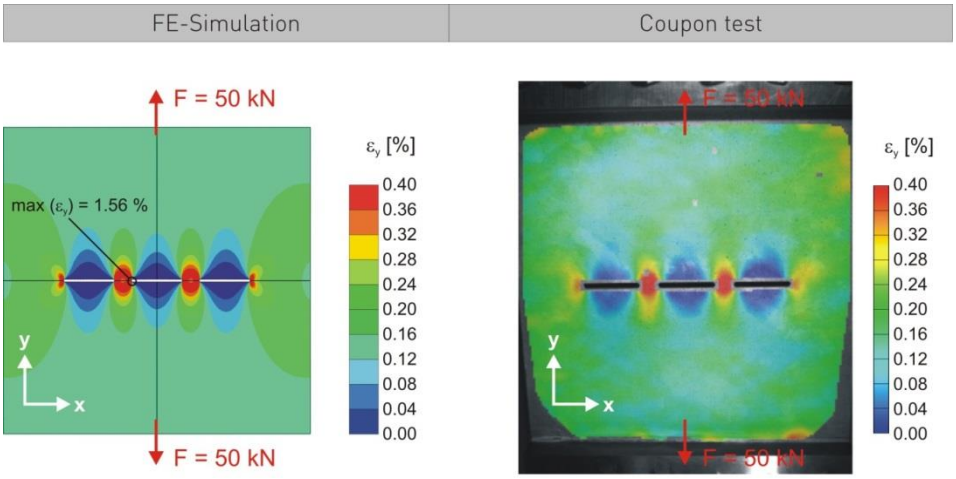

Figure 38: Comparison of the strain ε_y determined in FE-simulation and in coupon test

3.4.2 Fatigue tests (IFL)

Based on the FE-analysis and considering the fracture mechanic aspect all AFCIN partners decided to pass the 90° coupon tension tests. Therefore, only 3 specimens with 0°- and 45°- slits are tested and 3 specimens by shear load. During the fatigue tests ultrasonic testing is executed every 15000 load cycles. The aim of the testing is to detect and to trace delamination and/or cracks.

Tension tests

Depending on the defined fatigue loads pre-tests are carried out to test the measuring equipment and to check the prediction against the real test behavior. After that a static test up to limit load (LL) is performed. After finishing 60000 load cycles a further static test is executed. So, the results can be checked to find out any changes during an assumed airplane life. **Figure 39** shows the principle test set-up into the 1 MN Instron Wolpert test machine. For test set-up integration into the test machine 2 vertical supports will be used. After clamping the set-up, the supports will be replaced.

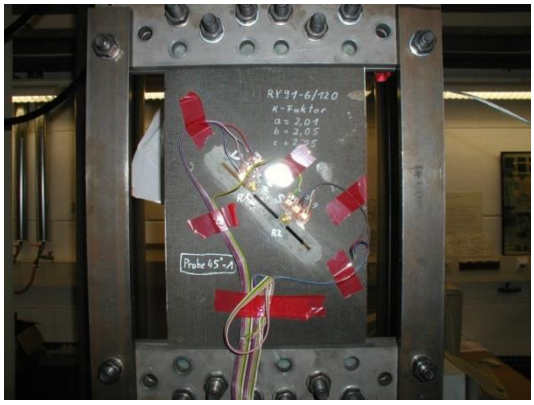

Figure 39: Principle test set-up of tension tests (left), additional supports for integration into the test machine (right)

0° test specimen The LL of this kind of specimen is 4.77 kN and the fatigue load amounts 3.84 kN. The maximum strain at LL amounts 3.82E-04 and obviously no changes of the specimen behavior can be noticed after 60000 load cycles. For this reason all partners decided to increase the load up to a corresponding strain level of nearly 2.70E-03. The test sequence was repeated with the new load level of 36 kN. 45° test specimen The LL of this kind of specimen is 26.57 kN and fatigue load amounts 21.39 kN. Maximum strain at LL amounts 1.00E-03 and so no changes will be expected after 60000 load cycles. For this reason all partners decided to increase the load up to a corresponding strain level of nearly 2.70E-03. Thickness of panel 3 is less than panel 1 and 2; therefore fatigue load is reduced to obtain a nearly same strain level. Orientation of the strain gauge channels are shown in **Figure 40**. Rosette 1 locates on the left side, rosette 2 on the right side.

The principle strain vs. time history is shown in **Figure 41** for the new manufactured specimen 1. The target strain of 2.70E-03 is reached by strain gauge tension direction (cannel Ros1_b). The strain vs. time history after 60000 load cycles is shown in Figure 5. There are significant changes detectable. Maximum strain amounts only 1.10E-03 due to delamination and combination of slit angle and load direction.

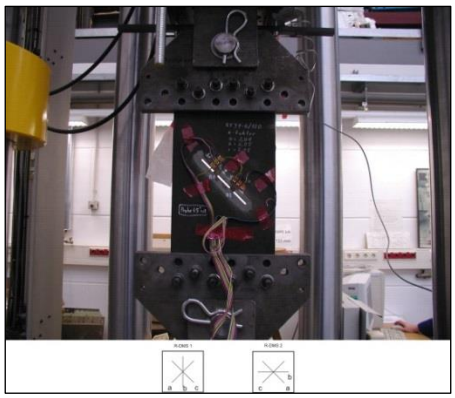

Figure 40: Orientation of the strain gauge channels

For 2nd and 3rd plates same strain history can be found. There is also a visible damage at specimen 2. The crack growths from the lowest slit (right side) upwards to the middle slit. Ultrasonic testing confirms results coming from strain gauges.

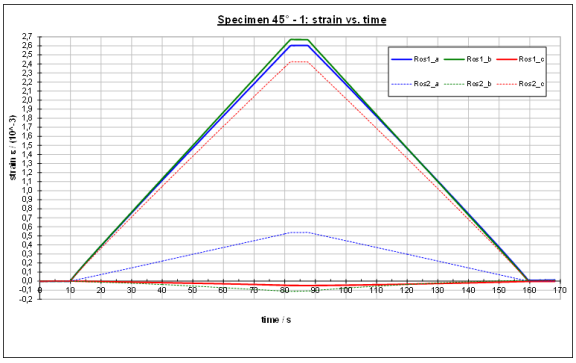

Figure 41: Strain history of specimen 45° - 1

Shear tests

Figure 42 shows the 250 kN test machine "PApS". On one side 2 rosette strain gauges are applied, on the other side there is a stochastic pattern for the optical measurement system "ARAMIS".

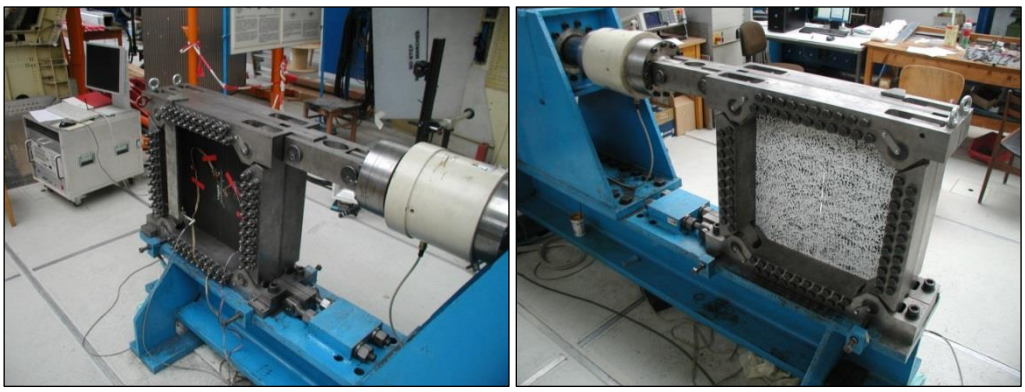

Figure 42: Test machine "PApS" with assembled test panel

The orientation of the strain gauge channels are shown in **Figure 43**. Rosette 1 locates on the left side, rosette 2 on the right side.

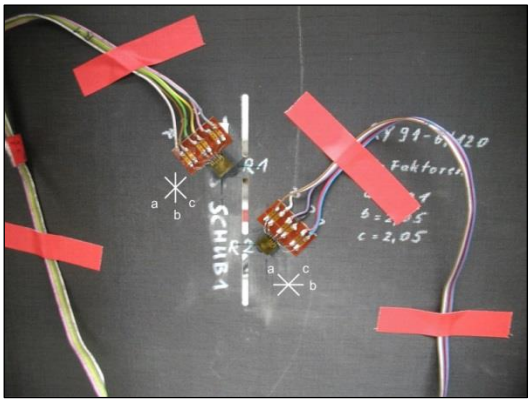

Figure 43: Orientation of the strain gauge channels

The LL of this specimen is 46.03 kN and the fatigue load amounts 37.05 kN. It can be seen from the strain vs. force and strain vs. time curves. There is a nonlinear behavior clearly noticeable. From about 13 kN panel buckling begins. And so the behavior is explainable. Channel Ros2_b is parallel to the cylinder axis and changes its behavior during the test due to buckling.

3.5 Flap test (IFL)

According to the calculations bending test load is 51.8 kN and torsion test load amounts 20.2 kNm. For the test set-up the flap locates in the principal axis and the shear centre from the calculations is used for the test rig. Pre-tests confirm the statements referring the variation of the stiffness and shear centre found in calculations before. Thus, there is no separated bending and torsion load case. Finally, only one load case is executed, a combined tension-torsion load case. The test load is 51.8 kN for the static test. Due to the combined load case all AFCIN partners decided to execute the fatigue test with a load of 30 kN.

3.5.1 Manufacturing

Manufacturing was performed by EADS-IW, now Airbus Group Innovations.

3.5.2 Test set-up

The test set-up is shown in **Figure 44**. The load introduction is realized by two 63 kN hydraulic cylinders (labeled F4 and F3) and a load introduction beam made of wood and steel. Cylinder F4 locates at the LE, F3 at the TE. 9 strain gauges rosettes are applied. Additionally to the displacement sensors of the cylinders, 4 inductive displacement transducers are used to measure the flap deformation. Their position is shown in **Figure 45**.

Figure 44: Test set-up of the flap test

Figure 45: Position of the displacement transducers

The clamping is realized by a fixed bearing (blue steel parts in **Figure 44**) and a moveable bearing (red brown steel parts). The flap lies inside a wooden beam supported by U-steel sections. The data acquisition system MGCPlus by firm Hottinger Baldwin Meßtechnik (HBM) is used for all static tests.

The Instron Labtronic 8400 controller is used to control the test in static and fatigue test case. The cables from the strain gauges are mounted by tape at the flap surface and are laid through the wooden beam to a junction box. This box is connected to the data acquisition system. **Figure 46** shows the strain gauges on the upper flap side for example.

3.5.3 Test results

Due to the combined load case a comparison between test results and FE-analysis is not really constructive. A not existing load introduction rib into the flap, the test set-up with a lot of mechanical joints and the load case itself cause a higher deformation than expected. Both hydraulic cylinders have the same distance to the estimated shear centre but the cylinder displacement differs by nearly a factor 1.74. So, the estimated shear centre is not the real one. By neglecting the displacement off-set the displacement history is shown in **Figure 47**. Cylinder F4 displacement is larger than F3 displacement. It results from a large leading edge deformation due to missing an additional rib. During the test the large LE deformation is clearly visible. There is also a larger deformation resulting by the test set-up. After the test a 0.62 mm displacement off-set of cylinder F4 is remarkable. It results from the settlement due to load.

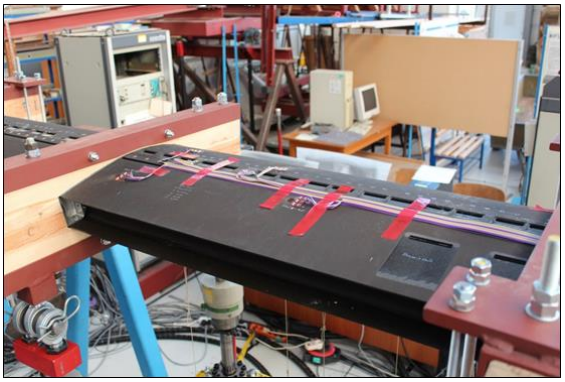

Figure 46: strain gauges on the upper flap surface

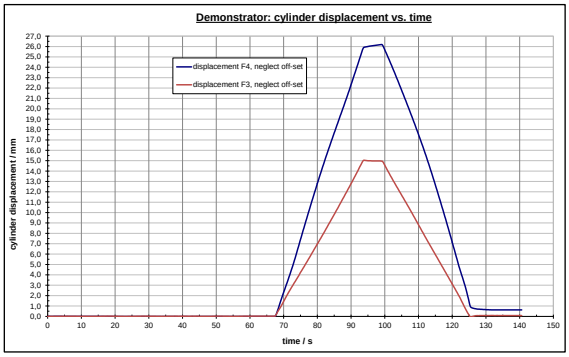

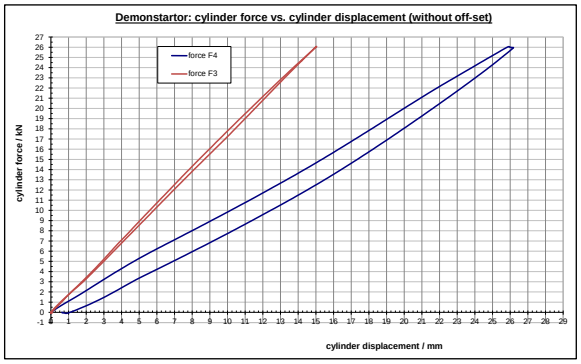

Figure 47: Cylinder displacement history and **Figure 48:** Force vs. displacement history

The force vs. displacement (without displacement off-set) history is shown in **Fehler! Verweisquelle konnte nicht gefunden werden.**. The yielding of cylinder F4 signal at maximum load results from the weak LE and the controller interaction of the both hydraulic cylinders.

3.6 Mock-up Demo (ILK)

An exhibition model of the flap including the AFC system has been developed and to show the design and assembly configuration as well as the functionality. Therefore a representative part of the flap has been chosen for the exhibition model to visualize the functionality of the AFC-system (see **Figure**

49). Most of the main structural components of the flap like the skins (A), the C-spar (B) as well as the spar box (D) has been made of carbon fibre reinforced plastic (CFRP) to give an impression of the real design within an aircraft, where these components are presumably made of CFRP. In contrast to that, the leading edge (F) as well as the Z-spar (E) has been made of transparent polycarbonate (PC) to have a better view on the main functional components of the AFC structure (C), which have been made of nontransparent polyamide (PA) and polyphenylene sulfide (PPS).

The manufacturing of the CFRP-components as well as the transparent PC-components required the design and realization of tools. **Figure 50** exemplarily shows the manufacturing of the tool for the leading edge made of PC. At first a master form has been milled out of a polyurethane block (PUR). Afterwards the tool has been laminated within this master form. This tool defines the shape of the leading edge, which is realized by forming a pre-heated PC-sheet on this tool.

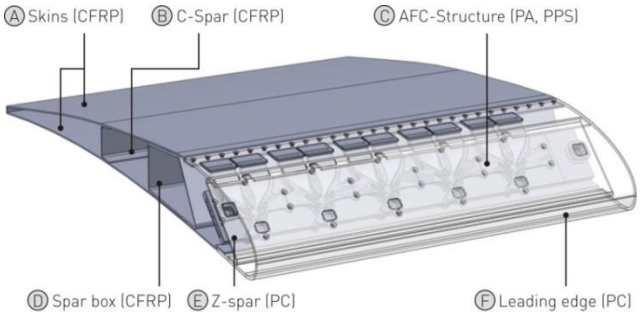

Figure 49: Final design of the flap exhibition model

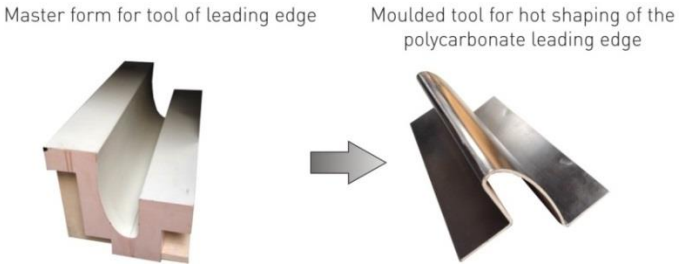

Figure 50: Realization of manufacturing tools

All components of the exhibition model are joined by riveting and bonding, which are established joining technologies within the aircraft industry. The finally assembled exhibition model of the flap with the AFC-system is shown in **Figure 51**.

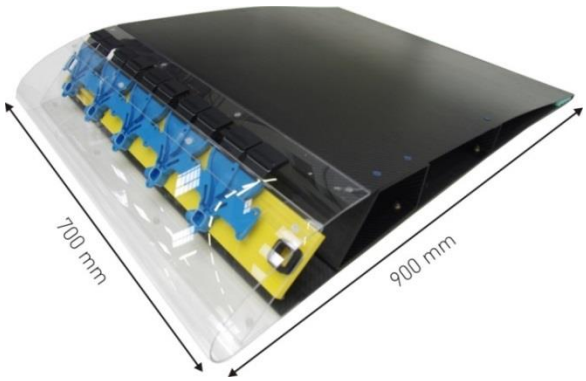

Figure 51: Exhibition model of the flap with AFC-system

4. Potential impact, dissemination and exploitation of results

4.1 Potential impact

Active flow control (AFC) is a means to achieve better and/or higher aerodynamic performance. In this case AFC has been applied to the flap, i.e. better high lift performance is envisaged. Such better high lift performance may be used to reduce the size of the flap (as done here) or e.g. to achieve shorter runway length etc.. It may even been used for steeper descend in order to reduce noise etc. From this point of view the potential impact regards environmental effects in a wide sense.

Whether such benefits are achieved by the design, which combines both approaches in AFCIN and FloCoSys is only measurable in an overall analysis, which was not subject to the project AFCIN. Locally, the size and weight of the flap has been reduced drastically, but whether this means a real overall benefit is questionable, taking into account the weight and cost of the entire system needed for this purpose.

The project did a large step forward in the sense that this project provided a realistic structural concept plus sizing and validation via testing for a flap of this kind. From this point of view it is a real step because it brings further details which are not achieved by a pure aerodynamic and/or system approach.

4.2 Dissemination

Dissemination took place within the CleanSky Consortium by keeping the industrial partners informed at each stage. Therefore, the main stakeholders are very well informed about the structural design which was developed and tested in this project.

Besides this direct link to industry, partners together with Airbus Group Innovations will present a paper "**Active Flow Control Integration into a CFRP Flap**" at the 2014 German Aerospace Congress (DLRK 2014). It is the intention of the authors to submit this paper to the CEAS Journal for refereed journal publication after the congress.

Individual partners will publish e.g. methods developed for the purpose of this project in further papers.

4.3 Exploitation of results

All partners directly involved in this project are university institutes. Therefore, an industrial exploitation cannot be made by the partners themselves. But, the partners will use the results in several ways, namely:

- In general, the three partners are in a very good position to join further projects (European or others) in the area of structural design; especially on active flow control.
- The structural design, calculation and manufacturing in the project are mainly performed with aviation certified tools and programs. This allows a fast adaption of the project results in industrial applications by means of certification requirements.
- A fast and efficient pre-design and optimization methodology has been developed in the project. By using fast, efficient and parametric numerical tools this process chain can also be applied to other structures like airplane wings or the development of new wind turbine rotor blades. The method can be extended modularly to consider other design aspects like stability or aeroelastic effects.
- In the frame of the German Collaborative Research Centre 880 other way to achieve active high lift are investigated. But, several points can be learned from AFCIN and will therefore allow to be successful in the next steps of the program.
-

5. Address and contact details

Institute of Aircraft Design and Lightweight Structures (Institut für Flugzeugbau und Leichtbau)

TU Braunschweig

Hermann-Blenk-Str. 35

D-38108 Braunschweig

Prof. Dr.-Ing. Peter Horst (p.horst@tu-bs.de) and

Dr.-Ing. Torsten Fabel (t.fabel@tu-bs.de)

Institute of Aerospace Engineering (Institut für Luft- und Raumfahrttechnik)

Chair of Aircraft Engineering (Lehrstuhl für Luftfahrzeugtechnik)

TU Dresden

Marschnerstraße 32

D-01062 Dresden

Prof. Dr.-Ing. Klaus Wolf (klaus.wolf@tu-dresden.de) and

Dipl.-Ing. Martin Rädel (martin.raedel@tu-dresden.de)

Institute of Lightweight Engineering and Polymer Technology (Institut für Leichtbau und Kunststofftechnik)

TU Dresden

Holbeinstr. 3

01307 Dresden

Prof. Dr.-Ing. habil. Prof. E.h. Dr. h.c. Werner A. Hufenbach and

Dr.-Ing. Andreas Ulbricht (andreas.ulbricht@tu-dresden.de)

6. References

[Bau12] Bauer, M. (2012). *SFWA-ITD report DT-FA-AFC D02 Pre-design analysis.* Berlin: TU Berlin.

[Kal06] Kaletta, P. (2006). *Ein Beitrag zur Effizienzsteigerung Evolutionärer Algorithmen zur optimalen Auslegung von Faserverbundstrukturen im Flugzeugbau.* Dresden: PhD thesis.

[Mac11] Machunze, W. (2011). *Weight estimation process for AFC approach.* Ottobrunn: EADS IW.

[Pat06] Paton, R., Hou, M., Beehag, A., & Falzon, P. (2006). A Breakthrough in the Assembly of Aircraft Composite Structures. *Proceedings of the 25h International Congress of the Aeronautical Sciences.* Hamburg: ICAS.

[See11] Seeger, J., & Wolf, K. (2011). Multi-objective design of complex aircraft structures using evolutionary algorithms. *Proceedings of the Institution of Mechanical Engineers, Part G: Journal of Aerospace Engineering* , 1153-1164.

[See07] Seeger, J., & Wolf, K. (2007). Structural optmization of adaptive airfoils using evolutionary algorithms. *Proceedings of the 1st CEAS European Air and Space Conference.* Berlin.

[Uri08] Urik, T., & Malis, M. (2008). Innovative Composite Structures for Small Aircraft. *Proceedings of the 26th International Congress of the Aeronautical Sciences.* Anchorage: ICAS.